Research Article

SOHAG JOURNAL OF SCIENCES

https://doi.org/10.21608/sjsci.2023.225470.1102

Optical Non-linear Characterization of V_2O_3 for Applications in Intensive Optical Radiation Systems

E. Kh Shokr[1], Sh. A. Elkot[1], Moumen S. Kamel[2,*], H. M. Ali[1]

[1]*Department of Physics, Faculty of Science, Sohag University, Sohag 82524, Egypt*
[2]*Department of Chemistry, Faculty of Science, Sohag University, Sohag 82524, Egypt*
[*]*Email: mim_chem2@yahoo.com*

Received: 1st August 2023**, Revised:** 26th September 2023, **Accepted:** 27th September 2023
Published online: 6th October 2023

Abstract: Vanadium oxideV_2O_3 thin films were synthesized by sol-gel spin coating method, and investigated by XRD, FE-SEM, EDAX, and UV-Vis- NIR spectroscopies. XRD and EDAX analysis has confirmed that the initial powdered orthorhombic V_2O_5 compound dissolved in H_2O_2 solution, heat treated at ≈ 70 ^{0}C and spin-coated has been transformed into monoclinic V_2O_3- phase thin films, resulting in free V^{3+} ion Formation. The morphology and optical analysis of the obtained films revealed that the grain size increases, and the gap energy decreases while the static refractive index changes, passing through a maximum value at 350 nm. The changes in non-linear refractive index n_2, third-order polarizability $\chi^{(3)}$, and F-function with light energy consist of the two-photon absorption and intensity-dependent refractive index conditions of optical non-linear characteristics. The maximum values of $7.67x10^{-11}$ and $5.08x10^{-12}$esu attained at the film thickness of 350 nm of n_2, $\chi^{(3)}$, respectively as a result of the compromise of different factors, such as the bound oxygen bonds and free ions, refractive index, localized state density, and number of crystallites, are better than the corresponding reported results for some oxide, chalcogenide, and organic materials.
Keywords: vanadium oxide thin films, sol gel-spin coating, XRD, EDAX, ESM, linear/non-linear optical properties.

1. Introduction

Vanadium oxide thin films are widely used in research and technology due to their unique qualities, which include strong chemical and thermal stability, thermoelectric and thermo chromic capabilities, and an adjustable band gap due to their multiagency [1-3]. It can form a large number of oxide compounds, which qualifies it to be used in a variety of applications [4]. Among these, the vanadium Magnéli phases are a series of stoichiometric compounds with V_nO_{2n-1} compositions, where n = 3, 4,... It is bordered by vanadium trioxide (V_2O_3), which is an oxide in which oxygen is present in the ratio of three atoms to two of other elements, and vanadium dioxide (VO_2), in which the vanadium valence is, respectively, 3 and 4 [5].

Varying the conductance of vanadium oxide compounds between the semiconductor and metal states provides the basis for electronic devices such as electronic switches, logic and memory units, and sensors [6, 7]. The mixed phases VO_x (VO_2, V_2O_3, and V_2O_5) of both amorphous and polycrystalline thin films are preferred for uncooled microbolometers in IR imaging applications [8-11].

Transition metal oxide thin films are promising nonlinear optical materials due to their high refractive index and localized electrons based on Miller's rule [12, 13]. The interaction of the electromagnetic radiation with the materials, which differs according to the radiation intensity, can result in electron-hole pair generation, charge in the lattice parameters [14, 15] and phase transformation (crystalline to amorphous and vice versa) [16-21]. Such an effect significantly influences both the charge density and length of the possible formed dipoles, which are essential contributing factors to polarization. This polarization becomes non-linearly proportional to the electric field when the material is exposed to highly intensive optical radiation like that of a laser. This leads to anharmonic responses in the medium, causing the non-linear effects to appear and dominate.

The non-linear refractive index n_2 and the third order of non-linear susceptibility $\chi^{(3)}$ are important parameters utilized to achieve optically limiting behavior and are used in a variety of applications [22–25]. The increased values of n_2 and $\chi^{(3)}$ enhancing can be realized by different factors, such as the polarizable bond density and their orientations concerning the induced electric field, the material compactness (material density), the bond length of polarizable species, and the density of localized states [26]. Vanadium oxide is believed to be a good candidate for applications in highly intensive radiation systems because of the bound oxygen bonds and free ions having high polarizability in the oxide matrix [27] and the existence of more than one electron in V_2O_5 or V_2O_3 oxides, which results in the formation of both short and long V-O bonds, causing polarization between them [25, 28].Therefore, vanadium oxide compounds could be characterized by their high refractive nonlinearity and 3rd-order nonlinear optical susceptibility [4-5, 29- 30].

Despite numerous studies of the NLO properties of metal-doped or un-doped V_2O_5 [29- 32], no results can be attained for the NLO properties of the V_2O_3-phase of vanadium oxide synthesized by the sol–gel spin coating method. In this work, the structural and optical characteristics of V_2O_3 thin films synthesized by the sol-gel spin-coated method have been investigated. Both linear and non-linear parameters influenced by the film thickness have been determined, discussed, and

compared with literature results.

2. Experimental

2.1. Thin film preparation

V_2O_3 thin films with thicknesses of 269, 350, 420, 558, and 620 nm were formed on glass surfaces, and 620 nm on Si-sheets were created using the sol-gel spin coating process. 0.5 g of 99.5% purity V_2O_5 powder was mixed in 30 ml of a 15% solution of H_2O_2 with rapid spinning (1000 rpm) till the mixture became red-brownish. After 30 minutes in a water bath at 70°C, the solution turned into a gelatinous solution, generating V_2O_3 gel.

The gel's viscosity is affected by the water bath heat and heating time. The films were deposited on glass and single crystal silicon (Si) substrates, which were thoroughly cleaned by washing them in an ultrasonic cleaner instrument (VGT-1613 QTD) with an internal volume of 2000 mL and a digital timer. A small amount of gel had been spin-coated on glass and Si substrates at 800 to 1200 rpm, depending on the needed film thickness. The films were then heated in the atmosphere at 150 ^{0}C for 1 hour to dry. The resultant films are green-yellow in hue, indicating a V^{+3} oxidation state. The thicknesses of the deposited films were determined by the weight method according to the following equation:

$$d(nm)=\frac{m}{\rho A}x10^7 \quad (1)$$

where, m is the film mass (g), ρ vanadium oxide density, and A is the film area (1.5x 3.2 cm^2).

2.2. Investigation techniques

The crystallographic structure of the formed films on glass substrates was studied using a Philips X-ray diffract meter (model PW1710) with Cu as the target and K_α as the filter, λ=1.541838 A^0. The x-ray diffract meter operates at 40 kV and 30 mA, with a 20/min scanning speed. The diffraction scan measured between 10 and 80^0 (2θ). Field-emission scanning electron microscopy (FE-SEM) via a JSM-6100 microscope with a 30 kV acceleration voltage was used to examine the surface topography of the films produced on glass substrates. The chemical structure of a 620 nm thick layer formed on Si-substrates has been investigated through dispersive analysis of an x-ray (EDAX) unit attached to the FE-SEM (EDS unit, HNU-5000).

The optical spectra of transmission T and reflection R were recorded at ambient temperature with a computer-programmable double beam spectrophotometer model Jasco-570 (Japan) at normal incidence and a scan speed of 400 nm/min in the wavelength range 200-2500 nm.

The effect of different thicknesses on the nonlinear optical parameters of V_2O_3 films will be studied to identify the best thickness to be employed as a highly intensive radiation system.

3. Results and discussion

3.1 Structural and surface morphology analyses

XRD patterns of the initial V_2O_5 powder and sol-gel spin coated thin films are depicted in Figure 1. As shown for the powdered material, there are different peaks at (2θ) = 15.4, 20.4, 21.79, 26.89, 31.06, 32.43, 34.35 and 41.41^0 corresponding to the orthorhombic V_2O_5 polycrystalline lattice, according to JCPDS file (card no. 77-2418) with lattice parameters a=11.51 A^0, b=3.564 A^0 and c=4.368 A^0 [33-35]. The most intensive (110) peak refers to the preferred crystallization direction. However, XRD patterns for the deposited thin films reveal three weak peaks only at 2θ = 24.963, 33.275 and 41.685^0, which are embedded in highly amorphous matrix and assigned to the monoclinic V_2O_3 with lattice parameters a= 8.6 A^0, b= 5.002 A^0, c= 7.255 A^0 and β = 140.17^0 according to the JCPDS file (card number 96-153-9771) [36]. This monoclinic structure refers to the film oxygen deficiency (V_2O_{5-x}), where x= 2 [37-39] leads to the formation of V^{3+} instead of V^{5+}.

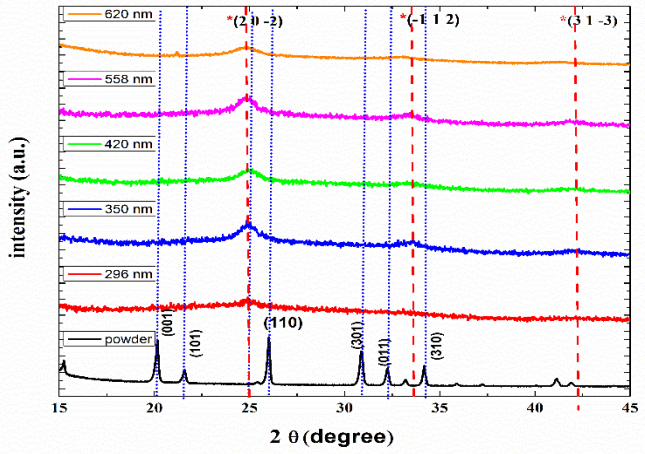

Fig.1: XRD diffractogram of the Vanadium oxide thin films with different thicknesses deposited on glass substrates.

The crystallite size of V_2O_5 powder and thin films were measured by using the FWHM of the preferred crystallization (110) and (20 -2) peaks, respectively, employing the following Debye Scherrer's formula [40, 41].

$$D=\frac{0.94\,\lambda}{\beta\,cos\,\theta} \quad (2)$$

where D is the grain size, λ is the X-ray wavelength employed, β is the angles of the line's width at half-maximum intensity in radians and θ is Bragg's angle. The formula that comes next [40, 41] may be used to calculate the dislocation density (δ), which provides further information about the amount of defects in the films.

$$\delta=\frac{1}{D^2} \quad (3)$$

while the number of crystallites per unit area can be calculated by the following relation [40, 41]:

$$N=\frac{t}{D^3} \quad (4)$$

where t is the film thickness.

The calculated D, δ and N values are listed in Table 1. As shown, the crystallite size D increases while the dislocation density δ and the number of crystallites N decrease by increasing the film thickness.

Table 1: The variations of the crystallite size D, dislocation density δ, and number of crystallites per unit area of vanadium oxide with film thickness.

Film thickness, t, nm	D (crystallite size) nm	dislocation density (δ) nm^{-2}	number of crystallites N, nm^{-2}
V_2O_5 powder	62.564	0.0003	0.002
269	3.304	0.0916	13.858
350	6.741	0.022	1.633
420	8.408	0.0141	0.841
620	9.677	0.0107	0.552

SEM images of the deposited films 269, 350, 420 and 620 nm thick are given in Figure 2. As shown, randomly separated tinny grains in the highly amorphous matrix are observed, especially for relatively thinner films. We believe that the probably existed voids and shanks in the thinner films have been formed due to the random distribution of material particles during the spin coating process. Increasing the film thickness noticeably improves the sample surface homogeneity. The grain's shape becomes clearer, and their size (in the micrometer scale) increases with the film thickness.

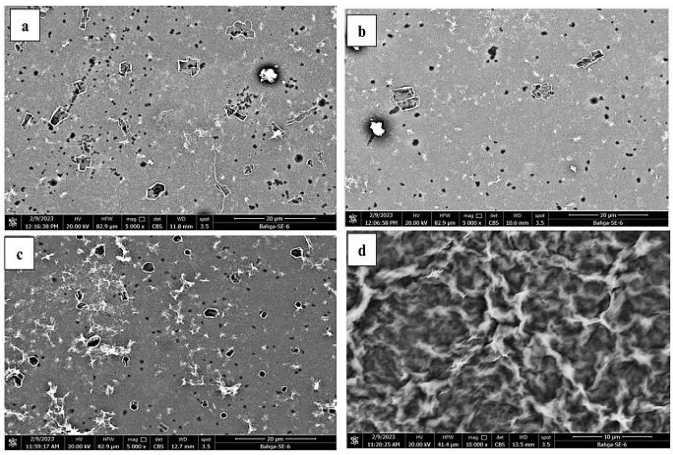

Fig. 2: SEM morphology analysis of V_2O_3 thin films on glass substrates with different thicknesses (a) 269 nm (b) 350 nm (c) 420 nm (d) 558nm.

X-ray (EDAX) analysis depicted in Fig. 3 for a V_2O_3 thin film of 620 nm thick deposited on a Si substrate as an example indicates that films are composed only of V, and O, confirming that the films are free from impurities. The calculated O/V ratio was about ≈ 1.59. This indicates that the formula V_2O_{5-x} corresponds to the V_2O_3–compound, which is consistent with the result of X-ray analysis.

3.2 Optical characterization

The measured transmission T and reflection R spectra (Fig. 4) were utilized to calculate the absorption coefficient α, the extinction coefficient k, and the refractive index n using the following equations [42-44].

$$\alpha = \frac{2.303}{d}\log\left[\frac{(1-R)^2}{T}\right] \quad (5)$$

$$K = \frac{\alpha\lambda}{4\pi} \quad (6)$$

$$n = \left(\frac{1+R}{1-R}\right) + \left[\left(\frac{1+R}{1-R}\right)^2 - (1+K^2)\right]^{\frac{1}{2}} \quad (7)$$

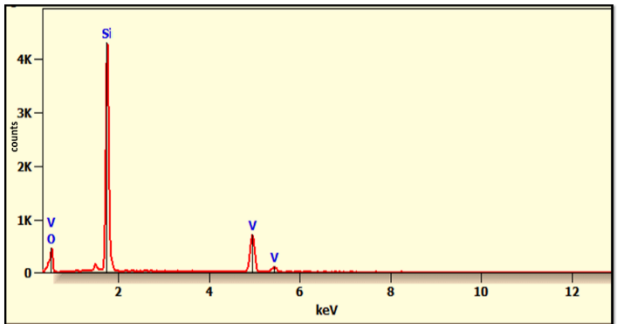

Fig. 3: EDAX elemental analysis of V2O3 thin film of 620 nm thick deposited on Si substrate.

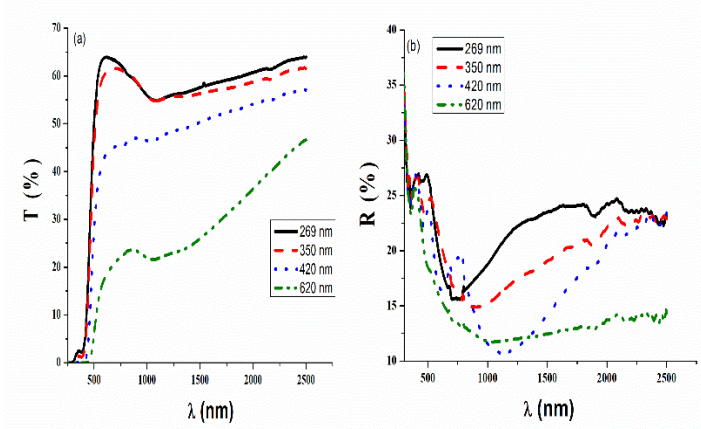

Fig.4: The optical transmission and reflection of as deposited V_2O_3 thin films of 269, 350, 420 and 620 nm thick

Besides, the localized states width (known by Urbach energy Eu) can be estimated using the following relation [45],

$$\alpha=\alpha_0\exp(h\upsilon/E_u) \quad (8)$$

In the range of normal dispersion of the refractive index n, at which n increases with increasing hυ, the energy dependence of the refractive index is represented by the following relation [46].

$$(n^2-1)^{-1} = \frac{E_o^2-(h\upsilon)^2}{E_o E_d} \quad (9)$$

Fig. (5) gives the spectral variation of lnα vs. hυ and $(n^2-1)^{-1}$ vs. $(h\upsilon)^2$. It is clear that α increases while n decreases over the whole considered spectral range with increasing film thickness. The calculated value of E_u, which increases with film thickness are given in Table (2). In the ≈ 500- 700 nm range of the wavelength λ, n decreases with λ- increase, manifesting a normal dispersion behavior. The calculated static refractive index n_0 (n at hυ=0) slightly changes with the minimum value at film thickness of 350 nm (Table 2).

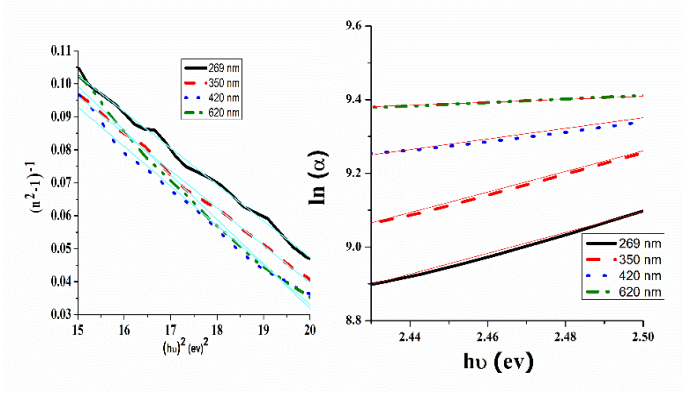

Fig. 5: Plots of $(n^2-1)^{-1}$ versus $(h\upsilon)^2$, and ln(α) versus (hυ) of vanadium oxide thin films.

Table 2: Values of non-linear refractive index n_2, 3rd–order non-linear susceptibility $\chi^{(3)}$ and the ratio of the energy gap E_g to the dispersion of non-linear absorption coefficient function F of vanadium oxide thin films of different thicknesses.

V_2O_3 film thickness (nm)	Eg ev	Eu ev	n_0	$\chi^{(3)}$, esu x10^{-12}	n_2, esu x 10^{-11}	F_{Emax}, (ev)	Eg/ F_{Emax}
269	2.4	0.32	2.17	3.34	5.27	4.36	1.4
350	2.35	0.36	2.18	5.08	7.67	2.67	1.3988
420	2.22	0.7	2.16	3.64	5.69	1.15	1.396
620	1.816	2.44	2.12	1.74	2.93	0.484	1.397

As described elsewhere [47], using the famous Tauc equation [48, 49] near the fundamental absorption edge, the values of the band gap energy E_g were determined and listed in Table (2). As shown, E_g decreases with the increase in film thickness. Both n_0 and E_g are crucial parameters that govern NLO behavior.

When an optical medium is impacted by an extremely intense electric field, its optical non-linearity behavior becomes dominant. As a result of the very intense laser field, electrons are displaced harmonically about their original centers, resulting in asymmetrical polarization that is non-linearly proportional to the radiated electric field [50].

The nonlinear refractive index n_2 and third-order optical polarizability $\chi^{(3)}$ are important factors for many nonlinear optical applications [51-54]. n_2 is an essential favorable parameter for nonlinear optical device performance [55, 56]. While $\chi^{(3)}$, which specifies third harmonic production, two-photon absorption, and intensity-dependent refractive index, is integral to the material validity definition for NLO devices. As a result, materials that have elevated maximum values of n_2 and $\chi^{(3)}$ are considered attractive for NLO systems.

Thus, depending on the strength of the incident light's electric field, the polarization P may be represented by the electric field power sequence inside [57,58].

$$P = \chi^{(1)}E + \chi^{(2)}E^2 + \chi^{(3)}E^3 \quad (10)$$

where $\chi^{(2)} = 0$ for optical isotropic glasses [4, 52], $\chi^{(1)}$ is the linear susceptibility.$\chi^{(1)}$ &$\chi^{(3)}$ and n_2 are related to the static refractive index through the following relations [59, 60] .

$$\chi^{(1)} = \frac{n0^2-1}{4\pi} \quad (11)$$

$$\chi^{(3)} = A(\chi^{(1)})^4 = \frac{A}{(4\pi)^4}(n_o^2-1)^4 \quad (12)$$

$$n_2 = \frac{12\pi\chi^{(3)}}{n_o} \quad (13)$$

Besides, the energy states that are coupled and the energy dispersion of non-linear absorption coefficient could be glanced by the following energy band structure dependent F-function [61- 63];

$$F = [(\frac{2h\upsilon}{Eg}) - 1]^{3/2}/(\frac{2h\upsilon}{Eg})^5 \quad (14)$$

The energy dependence of F-function is represented in Fig. (8). The calculated values of F_{Emax} are listed in Table (2). Based on the obtained results shown in Figs (6-8) and Table (2), the following conclusion could be drawn.

Both n_2 and $\chi^{(3)}$ manifest the same trend of spectral variation. They have maxima at approximately the same energy value of 1.825 eV. The values of these maxima increase with increasing film thickness from 269 to 350 nm and decline with further thickness increases to 620 nm. This change in n_2 and $\chi^{(3)}$ maximum values may be attributed to the change in the density and strength of the coupled species influenced by the film thickness.

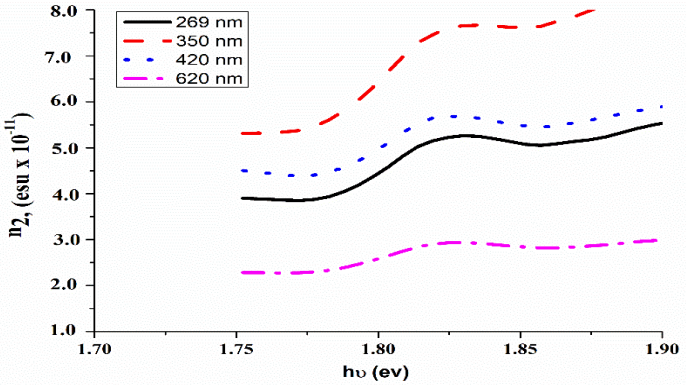

Fig. 6 Energy dependence of non-linear refractive index n_2 of V_2O_3 thin films with different thicknesses deposited on glass substrates.

The F-function of all films possesses the same spectral variation. It begins to rapidly increase at hυ>E_g/2 attaining a constant value at hυ>E_g, which is the characteristic of the two-photon absorption governed by the $E_g/2<h\upsilon<E_g$ condition [47]. The observed shifts to lower energy values are attributed to the decreased $E_g$values with increasing film thickness.

Besides, the value of E_g/F_{Emax} =1.4 obtained for all used films is consistent with many reported results of different compounds [64-67] and confirms the realization of the two-photon absorption condition.

The optical non-linear properties (NLO) of an optical material are essentially derived from the formed polarizable bond density, length, and orientation concerning the powerful induced electric field [68]. The NLO properties of the present vanadium oxide samples are assigned to the formed polarizable V-O bonds induced by the electric field and the free V-ions offered by the transformation of the initial V_2O_5 compound into the V_2O_3–oxide phase [69]. The strength of such NLO properties is dependent on the localized state density, which increases with film thickness [70]. Fig. (9) shows the variations of $\chi^{(3)}$ and the affecting factors on its maximum value, namely the static refractive index n_0 , the Urbach energy E_u and the crystallite

density with film thickness. As shown, n_0 increases with the film thickness increase due to the increase in material compactness influenced by crystallite size increase (Table 1) and contributes to $\chi^{(3)}$ enhancement, while the crystallite number N(nm^{-2}) decreases, inhibiting it. The highest values of $7.67x10^{-11}$ and $5.08x10^{-12}$ esu for n_2 and $\chi^{(3)}$, respectively (Table 2) are attained for the film thickness of 350 nm, at which these opposite NLO contributing factors are compromised. Table 3 gives a comparison of the present highest n_2 and $\chi^{(3)}$ values with the corresponding reported results for some other materials. The calculated ratios of the present n_2 and $\chi^{(3)}$ to the corresponding reported values have demonstrated that, excluding the n_2 and $\chi^{(3)}$ values of 1.9 x 10^{-8} and 5.46 x 10^{-7}esu for V_2O_5, respectively [31] which are significantly higher than the present n_2 and $\chi^{(3)}$ values, the present values of n_2 and $\chi^{(3)}$ are higher than the reported ones by ≈ 2.37-7.52x10^6 and 0.326 - 4.88 times, respectively.This refers to the application promise of the present V_2O_3 films in NLO systems.

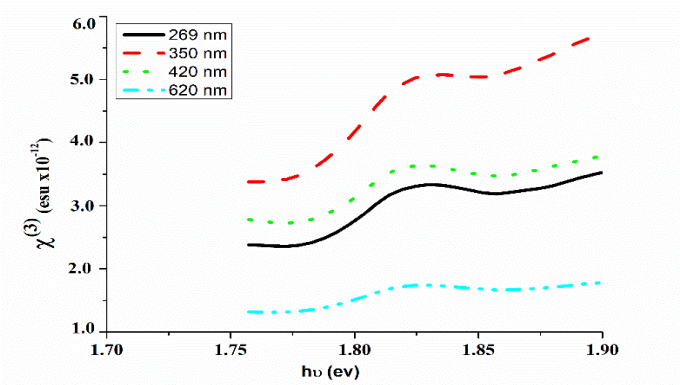

Fig.7 Energy dependence of third-order non-linear susceptibility $\chi^{(3)}$ of V_2O_3 thin films with different thicknesses.

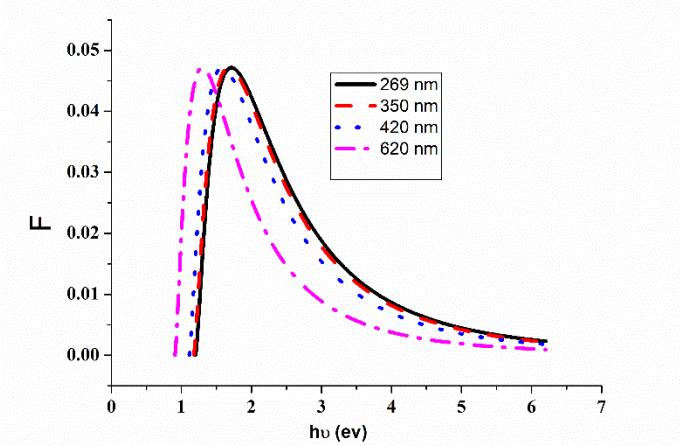

Fig. 8. Spectral variation of F-function for V_2O_3 films with different thicknesses deposited on glass substrates.

4. Summary and conclusion

V_2O_3 thin films were synthesized by the sol-gel spin-coating technique from the initial V_2O_5-powdered form and examined by XRD, FE-SEM, EDAX, and UV-Vis-NIR spectroscopies. It was revealed that the structure of the initial powdered samples is orthorhombic polycrystalline, while that of the thin films, has

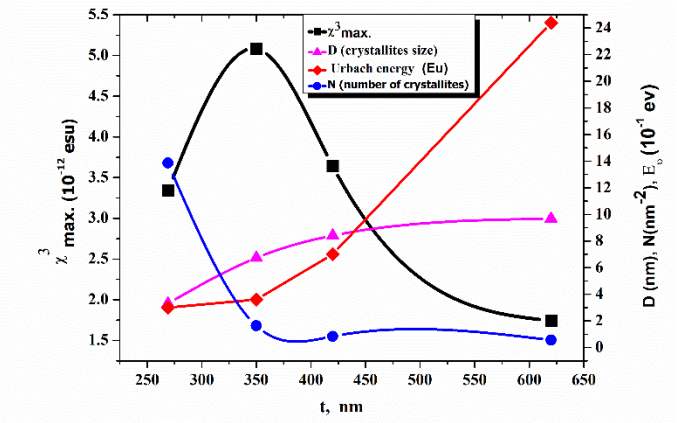

Fig. 9. Crystallite size D, Urbach energy E_u, number of crystallites per unit area N and, $\chi^{(3)}$ of vanadium oxide thin films of different thickness.

Table 3: compression of the present n_2& $\chi^{(3)}$ best maximum values with other reported results.

Material	Preparation method	n_2(esu)	$\chi^{(3)}$ (esu)	Ref.
V_2O_3	Sol-gel spin coating (350 nm)	$7.67X10^{-11}$	$5.08X10^{-12}$	Present work
$(CdO)_{0.99}Zn_{0.1}$	Thermal evaporation	$1.23x10^{-12}$	$5.73X10^{-14}$	[71]
MnO_2	conventional melt-quenching method	$5.08 X10^{-15}$	$6.36X10^{-13}$	[66]
$Ge_{20}Se_{75}In_5$	Thermal evaporation (1550 nm)	$1.02x10^{-17}$	$1.56x 10^{-11}$	[22]
$As_{40}S_{45}Se_{15}$	Thermal evaporation (1000 nm)	$3.24x10^{-11}$	$1.04x10^{-12}$	[23]
TT amino cyano N,N-dimethyl derivatives	Thermal evaporation (300 nm)	$1.10x10^{-12}$	$0.55x10^{-12}$	[47]
$(V_2O_5)_{0.94}Sn_{0.6}$	Thermal evaporation	$5.87x10^{-11}$	$4.19x 10^{-12}$	[30]
V_2O_5 thin films on MgO (100) substrates	PLD technique.	2.07×10^{-15}	3.03×10^{-11}	[29]
V_2O_5 thin film	sol-gel spin coating, (350 nm)	$1.9x10^{-8}$	$5.46x10^{-7}$	[31]
nanosized V_2O_5	Spray pyrolysis (Tann.= 550 ^{0}C)	$2.236x10^{-11}$	$2.266x10^{-31}$	[32]

tinny crystallite grains embedded in a large amorphous matrix, and corresponds to a monoclinic V_2O_3 phase. The values of the absorption coefficient α_{500} (0.84-1.2 x 10^4 cm^{-1}) at the solar maximum ($\lambda = 500nm$), refractive index n (2.17-2.12), and band gap energy (2.4 - 1.8 eV) found for the film thickness of 269-620 nm, respectively, confirming the high sensitivity of the

optical linear parameters to the film thickness. Besides, the variations of non-linear parameters n_2, $\chi^{(3)}$, and the F-function with energy have proved to verify the condition of non-linear characteristics. The maximum values of $7.67x10^{-11}$ and $5.08x10^{-12}$ esu of n_2, $\chi^{(3)}$ respectively, attained at a film thickness of 350 nm are the result of the compromised contributing (crystallite size, localized states, refractive index n_0, and free vanadium ions) and inhibiting (crystallite number N) factors.

In conclusion, the comparison of the present results with the corresponding reported ones of different oxide, chalcogenide, and organic materials indicates that the present results of NLO parameters could recommend the present V_2O_3 - thin films as a reasonable candidate for powerful optical radiation applications.

CRediT authorship contribution statement:

Author Contributions: For research articles with several authors, a short paragraph specifying their individual contributions must be provided. The following statements should be used "Conceptualization, methodology, software, validation, formal analysis, investigation, resources, writing—original draft preparation, project administration E. Kh Shokr, Sh. A. Elkot; data curation, project administration, software, Moumen S. Kamel; writing—review and editing, supervision, visualization H. M. Ali. All authors have read and agreed to the published version of the manuscript."

Data availability statement

The data used to support the findings of this study are available from the corresponding author upon request.

Declaration of competing interest

The authors declare that they have no known competing financial interests or personal relationships that could have appeared to influence the work reported in this paper.

Acknowledgments

All author thanks Sohag University for supporting this research.

References

[1] C. Prameela, M. Anjaiah, K.K. Murthy, K. Srinivasarao, *Appl. Phys.* 51 (2013) 6.
[2] R.T. R. Kumar, B. Karunagaran, V. S. Kumar, Y.L. Jeyachandran, D. Mangalaraj, S.K. Narayandass, *Mater. Sci. Semicond. Process*. 6 (2003) 543–546.
[3] E.E. Chain, *Appl. Opt*., 30.19 (1991) 2782–2787.
[4] U. Kürüm, R.M. Öksüzoglu, M. Yüksek, H.G. Yaglioglu, H. Çınar, and A.Elmali, *Appl Phys A*, 104 (2011) 1025–1030.
[5] R. Armando, D. D. Ramon, N. Kumar, S. Lysenko, and F. E. Fernandez, a*pplied physics*, 121 (2017) 235302.
[6] A.E. Owen, P.G. Le Comber, J. Hajto, M.J. Rose, A.J. Snell, *Int. J. Electro*, 73 (1992) 897.
[7] H. Pagnia, *Int. J. Electro*n, 73 (1992) 819.
[8] A. Subrahmanyam, Y. B. K. Reddy, C.L. Nagendra, *Appl. Phys*, 41(2008) 195108.
[9] J. Dai, X. Wang, S. He, Y. Huang, X. Yi, *Infrared Phys. Technol*, 51(2008) 287
[10] B.D. Gauntt, E.C. Dickey, M.W. Horn, *Mater. Res*, 24 (2009)1590.
[11] C. Venkatasubramanian, O.M. Cabarcos, D.L. Allara, M.W. Horn, S. Ashok, Vac. Sci. Technol.,A, 27(2009) 956.
[12] R. C. Miller, *Appl. Phys. Lett*., 5 (1964) 17.
[13] C. C. Wang, *Phys. Rev. B*, 2 (1970) 2045.
[14] S. J. Fonash, S. Ashok, and R. Singh, *Applied physics letters*, 39 (1981) 423-425.
[15] E. Grusell, S. Berg, and L. Andersson, *J. of The Electrochemical Society*,127 (1980)1573-1576.
[16] T. Nagase, Y. Umakoshi, and N. Sumida, *Materials Science and Engineering: A*, 323 (2002) 218-225.
[17] T. N. Agase and Y. Umakoshi, *Materials Science and Engineering:* A,343 (2003)13-12.
[18] R. Tarumi, K. Takashima, and Y. Higo, *Applied physics letters*, 81 (2002) 4610-4612.
[19] R. Qin, S. Su, J. Guo, G. He, and B. Zhou, *Nanostructured materials*,10 (1998) 71-76.
[20] H. Mizubayashi, N. Kameyama, T. Hao, and H. Tanimoto, *physical review* B,64 (2001) 054201.
[21] C. Suryanarayana, W. Wang, H. Iwasaki, and T. Masumoto, *Solid state communications*, 34 (1980) 861-863.
[22] I. Sharma, S. Tripathi, P. Barman, *Phase Transitions*, 87 (2014) 363–375.
[23] E.R. Shaaban, M.Y. Hassaan, M. Moustafa, A. Qasem, G.A. Ali, *Optik*, 186 (2019) 275–287.
[24] H. Abdelmaksoud, and F.A. Abdel-Wahab, *Scientific & Academic Publishing*, 8 (2018) 1-8.
[25] H. Zeyada, and M. Makhlouf, *Opt. Mater*, 54 (2016) 181–189.
[26] S. Ching-Fong, and W.Yuh-Kai, *J. Mater. Chem*, 8(1998) 833–835.
[27] S. Mansour, M. Hassaan, A. Emara, *Phys. Scripta*, 89.11 (2014) 115812.
[28] M. Makhlouf, *Sens. Actuators A: Phys*, 279 (2018) 145–156.
[29] L. Cui, R. Wang, and W. Wang, J. Korean *J. Mater. Res*, 31 (2021) 382-385.
[30] S. Yadav, S. Kumari, R. Bala, Gagandeep, R. Thakur, D. Mohan, *J. Materials Today: Proceedings*, 46 (2021) 5766-5771.
[31] G. Ravinder, C. J. Sreelatha, V. Ganesh, M.Shkir, M. Anis and P. C. Rao, *J. Mater. Res. Express*, 6 (2019) 096403.
[32] H. Khmissi, S. A. Mahmoud, A. A. Akl, *J. Optik - International Journal for Light and Electron Optics*, 227 (2021) 165979.
[33] K. Karthik, M. P. Nikolova, A. Phuruangrat, S. Pushpa, V. Revathi and M. Subbulakshmi, *J. Materials research innovations*, 1433-075X (2019) 1432-8917.
[34] R. Saravanan, V. K. Gupta, E. Mosquera, F. Gracia, J. *Mol Liq*, 198 (2014) 409-412.
[35] S. K. Jayaraja, V. Sadishkumarb, T. Arunc, P. Thangaduraia, J. *Materials Science in Semiconductor Processing*, 85 (2018) 122–133.
[36] D. P. Partlow, S. R. Gurkovich, K. C. Radford, and L. J. Denes, J. Appl. Phys. 70 (1991) 443- 452.
[37] Matthe-ur-Rahman, M. K. Alamgir, M. Z. Khan, R. H. Ahmed, H. Razzaq, *Arab J Sci Eng 43(2018) 407–413.*
[38] M. Nazemiyan, and Y. S. Jalili1, J. *AIP ADVANCES*, 3 (2013) 112103
[39] L. Gao, V. Wang, L. Fei, M. Ji, H. Zheng, H. Zhang, T. Shen, and K. Yang, *J. Cryst. Growth.* 281(2005)463-467.
[40] S. Subramanian, D. P. Padiyan, *J. Mater. Chem. Phys*, 107 (2008) 392–398.
[41] N. Benramdane, W. A. Murad, R. H. Misho, M. Ziane, Z. Kebbab, *J. Mater. Chem. Phys*, 48 (1997) 119–123.
[42] M.C.R. Castro, M. Belsley, A.M.C. Fonseca, M.M.M. Raposo, *Tetrahedron*, 68 (2012) 8147–8155.
[43] E. Genin, V. Hugues, G. Clermont, C. Herbivo, M.C.R. Castro, A. Comel, M.M. M. Raposo, M. Blanchard-Desce, *Photochem. Photobiol. Sci*, 11 (2012) 1756–1766.
[44] W. G. Spitzer and H. T. Fan, *Phys Rev*, 106 (1957) 882.
[45] F. Urbach, *Phys. Rev*, 92 (1953) 1324.
[46] S. Wemple, M. Jr. DiDomenico, *Phys.Rev.B, 3* (1971) 1338.
[47] E. Kh.Shokr, M. S. Kamel, H. Abdel-Ghany, M.ElRemaily, A.

Abdou, *J. Materials Chemistry and Physics*, 290 (2022) 126646.
[48] N.F. Mott, E.A. Davis, Electronic processes in non-crystalline materials. 2nd Ed. Oxford university press, 2012.
[49] J. Tauc, in Amorphous and Liquid Semiconductors, edited by J. Tauc (Plenum Press, New York, 1979), p. 159
[50] P. Sharma, and S. Katyal, *J. Appl. Phys*, 107 (2010)113527.
[51] E. A. Romanova, Y. S. Kuzyutkina, V. S. Shiryaev, S. Guizard, *Quantum Electron*, 48 (2018) 228.
[52] M. Diouf, A. B. Salem, R. Cherif, A. Wague, M. Zghat, *opt. Mater*, 55 (2016) 10-16.
[53] M. Diouf, A. B. Saiem, R. Cherif, H. Saghaei, A. Wague, *Appl. Opt*, *56* (2017) 163- 169.
[54] P. Sharma and S. Katayal, *Journal of Applied physics*,107 (2010) 113527.
[55] I. Sharma, S. Tripathi, P. Barman, *Phase Transitions*, 87 (2014) 363–375.
[56] H. Zeyada, and M. Makhlouf, *Opt. Mater*, 54 (2016) 181–189.
[57] P. Verghese, D. Clarke, *J. Appl. Phys*, 87 (2000) 4430–4438.
[58] A. Jilani, M.S. Abdel-wahab, A.A. Al-ghamdi, A. S. Dahlan, I. Yahia, *Phys. B Condens. Matter*, 481 (2016) 97–103.
[59]. H. Ticha, and L. Tichy, J. *Optoelectron. Adv. Mater*, 4 (2002) 381–386.
[60]. T. Wang, X. Gai, W. Wei, R. Wang, Z. Yang, X. Shen, S. Madden, and B. Luther-Davies, optical materiales express, 4 (2014) 1011- 1022.
[61] M. El-Nahass, H. A. El-Khalek, A.M. Nawar, *Eur. Phys. J. Appl. Phys*, 57 (2012).
[62] J. Stevels, Ultraviolet transitivity of glasses, Proceedings 11th International Congress Pure and Applied Chemistry, 1953, pp. 519–521.
[63] L. Petit, N. Carlie, R. Villeneuve, J. Massera, M. Couzi, A. Humeau, G. Boudebs, K. Richardson, J. *Non-Cryst. Solids*, 352 (2006) 5413–5420.
[64] F. A. Abdel-Wahab, H. Abdel Maksoud, International Journal of Optoelectronic Engineering, 8(1) (2018)1-8.
[65] I. Yahia, G. Salem, J. Iqbal, F. Yakuphanoglu, *Phys. B Condens. Matter*, 511 (2017) 54–60.
[66] S. Mansour, M. Hassaan, A. Emara, *Phys. Scripta*, 89 (2014), 115812.
[67] K.S. Abedin, *Opt Express*, 14 (2006) 4037–4042.
[68] I. Sharma, S. Tripathi, P. Barman, *Phase Transitions*, 87 (2014) 363– 375.
[69] S. Mansour, M. Hassaan, A. Emara, *Phys. Scripta*, 89 (2014) 115812.
[70] A. Andreas, I. Breuning, K. Buse, *Chem. Phys. Chem*, 6 (2005) 1544-1553.
[71] I. Yahia, G. Salem, J. Iqbal, F. Yakuphanoglu, *Phys. B Condens. Matter*, 511 (2017) 54–60.